

**QUANTIFYING THE TRANSITION FROM OCCASIONAL TO CHRONIC
COASTAL FLOODING**

A THESIS SUBMITTED FOR PARTIAL FULFILLMENT
OF THE REQUIREMENTS FOR THE DEGREE OF
BACHELOR OF SCIENCE
IN
GLOBAL ENVIRONMENTAL SCIENCE

MAY 2023

By

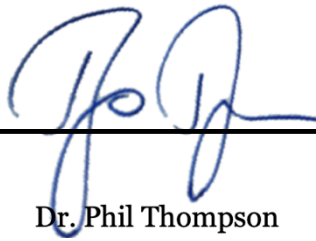
Kyra A. Leon

Thesis Advisor

Dr. Phil Thompson

I certify that I have read this thesis and that, in my opinion, it is satisfactory in scope and quality as a thesis for the degree of Bachelor of Science in Global Environmental Science.

THESIS ADVISOR

A handwritten signature in blue ink, appearing to read 'P. Thompson', is positioned above a solid black horizontal line. The signature is stylized and cursive.

Dr. Phil Thompson

Department of Oceanography

For all my friends in GES, who can always make me laugh when life gets hard, and
without whom this thesis would not have been completed.

ACKNOWLEDGEMENTS

Thank you to my advisor, Dr. Phil Thompson, for his guidance, encouragement, and wisdom throughout the completion of this project, and for making it fun and challenging. Thank you also for supporting me from day one, when I could not code a line in python, and for helping me to gain valuable skills that I will use throughout the rest of my life and career. Also, a big thank you to Dr. Glenn Carter for supporting my interest in physical oceanography and believing that someday I will get there. Finally, I would like to thank my friends in the GES program, who have supported each other throughout our academic careers in GES and the thesis process, and my parents, who made me calculate tip percentages at restaurants so I would grow up to enjoy math and problem solving.

ABSTRACT

Many coastal locations currently experience occasional instances of flooding. With rising global mean sea level, many locations will experience a shift in the frequency of flooding events. Coastal flooding threatens property and infrastructure, and growing instances of flooding threaten to displace significant portions of the global population currently living in coastal areas. In addition, decreased time between flooding events could negatively affect the time available to respond to damages. Meaningful adaptation and preparation for a changing flood regime is reliant on quantifiable data. The purpose of this study is to quantify the transition from occasional to chronic coastal flooding for locations globally. Using sea-level rise projections based on emissions scenarios and timeseries from a global set of tide gauges, we established a timeline for the transition across global locations. For an intermediate sea-level rise scenario, the median transition time was 35.71 years. However, the transition times for many islands and lower latitude locations was a decade or more shorter than the global median. Flooding is expected to increase in most locations, but islands and lower latitude coastal areas are the most threatened with the shortest projected transition times to chronic flooding conditions.

Keywords: Sea Level Rise, Coastal Flooding

TABLE OF CONTENTS

Acknowledgments	iv
Abstract	v
List of Tables	vii
List of Figures	viii
List of Abbreviations	ix
1.0 Introduction	10
1.1 Global Sea Level Rise	10
1.1.1 Regional Sea Level Rise	10
1.2 Coastal Flooding	13
1.3 Motivation	15
2.0 Methods	17
2.1 Selecting Tide Gauges	17
2.2 Determining Transition from Occasional to Chronic	17
2.2.1 Required Sea Level Rise	17
2.2.2 Transition Timeline	20
2.3 Non-Tidal Residuals	21
3.0 Results	22
3.1 Required Sea Level Rise	22
3.2 Transition Timeline	25
3.2.1 Non-Tidal Residuals	28
3.2.2 Islands and Continents	30
3.2.3 Latitude	31
4.0 Discussion	33
Appendix A: Tables	36
Appendix B: Figures	38
References	39

LIST OF TABLES

<u>Table</u>	<u>Page</u>
1. Median transition time by region and start year	28
2. Median transition time by region and start year	36
3. Median transition time, STD of predicted tide, and STD of non-tidal residuals by latitude	37

LIST OF FIGURES

Figure	Page
1. Locations of Selected Tide Gauges and Length of Record at Each Location	17
2. Example Time Series of Daily Maximum Sea Level and Δh	19
3. SLR Needed to Reach T_{chr} (Δh)	23
4. Correlation between Δt_{2020}	24
(a.) STD of Predicted Tide	
(b.) STD of NTRs.	
5. Number of Years Transition Time to T_{chr}	26
(a.) Starting in 2020 (Δt_{2020})	
(b.) Starting in 2050 (Δt_{2050})	
6. Correlation Between STD of Predicted Tide and STD of NTRS, and Transition Time (Δt_{2020})	29
7. Regional and Island Distribution of	30
(a.) Transition Time	
(b.) Standard Deviation of Predicted Tide	
(c.) Standard Deviation of Nontidal Residuals	
8. Distribution by Latitude of	32
(a.) t_{2020}	
(b.) STD of Predicted Tide	
(c.) STD of Non-tidal Residuals	
9. Tide Gauges Separated Into Regions	8

LIST OF ABBREVIATIONS

Abbreviation	Definition
GMSL	Global Mean Sea Level
SLR	Sea-Level Rise
GIA	Glacial Isostatic Adjustment
EWL	Extreme Water Level
T_{occ}	The threshold over which occasional flooding is likely to occur (more than 1 day of exceedances by mean daily maxima sea level)
T_{chr}	The threshold over which chronic flooding is likely to occur (more than 20 days of exceedances by mean daily maxima sea level)
Δh	The required change in sea level to transition from occasional to chronic flooding.
Δt_{2020}	The required time to transition from occasional to chronic flooding starting in the year 2020
Δt_{2050}	The required time to transition from occasional to chronic flooding starting in the year 2050

1.0 INTRODUCTION

1.1 Global Sea Level Rise

As climate change progresses, sea levels are expected to rise. Global greenhouse-gas emission rates dictate the severity of the warming and the rate of climate change. Climate change directly affects global mean sea level (GMSL) rise, caused by thermal expansion and glacial and ice sheet mass loss (Frederikse et al., 2020; Sweet et al., 2022). Since 1900, ice mass loss has contributed twice as much to GMSL than thermal expansion (Frederikse et al., 2020). Changes in terrestrial water storage are also known to contribute to changes in GMSL, however with increasing rates of thermal expansion and ice loss from the Antarctic and Greenland ice sheets, the contribution of terrestrial water storage to long-term future GMSL rise is negligible (Frederikse et al., 2020; Kopp et al., 2014). In the last 100 years, GMSL increased by 17 cm, with a notable acceleration in the rate of GMSL increase occurring around 1970, due to increasing ice mass loss from Greenland (Frederikse et al., 2020). Over the next 80 years, a mean increase in global temperature of 2 °C over preindustrial temperatures corresponds to a 50% probability of GMSL rise surpassing 0.5 m (Sweet et al., 2022). High emissions scenarios predict a potential increase of 3 °C to 5 °C, resulting in 80% to 99% probability of exceeding 0.5 m GMSL rise, and 5% to 25% probability that GMSL rise will exceed more than 1 m (Sweet et al., 2022).

1.1.1 Regional Sea Level Rise

GMSL is an important indicator of global change, but it does not account for regional variability, which may cause some locations to experience frequent coastal flooding sooner than expected from global change alone. Sea-level change differs regionally from GMSL for a variety of reasons. Regional variation in coastal sea level occurs due to steric sea level change, vertical land movement, and ice-mass loss

resulting in gravitational, rotational, and deformational changes over the globe (Vousdoukas et al., 2018, Frederikse et al., 2020). Sterodynamic sea level changes occur due to changes in circulation and density in the ocean, stemming from changing temperature and salinity that can be related to long-term climate trends or wind-driven variations associated with natural climate fluctuations (Gregory et al., 2019). In particular, the possible decline of the Atlantic meridional overturning circulation (AMOC) could contribute to higher rates of regional sea level rise on the east coast of the US (Krasting et al., 2016). Regional gravitational and deformational changes are caused by ice-mass loss to the ocean from glaciers and ice sheets (Frederikse et al., 2020). Both location and amount of ice mass loss affect regional sea level (Vousdoukas et al., 2018, Kopp et al., 2014). Locations nearest to areas with large amounts of ice mass loss tend to experience a decrease in sea level compared to the global average, while locations further away tend to experience an increase in sea level compared to the global average (Vousdoukas et al., 2018). The causes of vertical land movement vary based on location and occur due to many different processes, such as tectonic motion, withdrawal of groundwater, and compression and transport of sediments. (Miller et al., 2013). Together, sterodynamic changes, gravitational, rotational, and deformational changes, and vertical land movement are responsible for most regional variation in sea level rise.

By the end of the century, the South Pacific region is projected to experience the highest increase in extreme water level under RCP4.5, with the possible range of increase being 54cm-217cm (Vousdoukas et al., 2018). Extreme water level is defined as mean sea level added to the high tide water level and fluctuations due to waves and storm surges (Vousdoukas et al., 2018). Islands in the central Pacific are also likely to experience high SLR, and are expected to experience greater than average rates of SLR in the latter half of the century due to a projected increase in ice sheet mass loss (Kopp et al., 2014). For example, under RCP8.5, Honolulu, HI is projected to experience a likely increase of 0.6-

1.1 m by 2100 compared to a global average of 0.4–0.9 m (Kopp et al., 2014). Similar to the Central and South Pacific, the distance of Eastern Asia from most major ice sheets and glaciers will likely lead to more significant regional sea level rise (Kopp et al., 2014). Southeast Asia as a region is projected to experience a 37–79 cm increase in extreme water level (Vousdoukas et al., 2018).

The Atlantic Coast of the US and the coast of the North Sea in Northern Europe are also likely to experience greater than the GMSL rise by 2100 (Kopp et al., 2014). The projected change in regional sea level for the Atlantic coast of the US is 0.7-1.3m by 2100 under RCP8.5 (Kopp et al., 2014). This greater than global average increase is due to distance from the Antarctic ice sheet, lowering of the ground due to GIA and predominant soil composition, and potential changes in the Gulf Stream (Miller et al., 2013, Kopp et al., 2014). The North Sea is similar to the Atlantic US coast in proximity to Greenland but is exposed to less oceanographic sea-level rise (Kopp et al., 2014). Northern Europe is heavily glaciated, and many locations are projected to experience uplift due to GIA that will reduce the total sea level rise, or even lead to a decrease in sea level (Kopp et al., 2014). Due to these reasons, The North Sea is similar to the Atlantic US coast in proximity to Greenland but is exposed to less oceanographic sea-level rise (Kopp et al., 2014). For example, Stockholm, Sweden, is likely to experience sea level change of -0.4 to 0.8 m by 2100 (Kopp et al., 2014).

Many high latitude locations, such as in Alaska and western Canada, are projected to experience a sea level fall due to presence of glaciers and subsequently large rates of GIA (Larsen et al., 2005, Kopp et al., 2014). For example, Juneau, Alaska is projected to experience a decrease in sea level of 0.7-1.1 m by 2100 under RCP8.5 (Kopp et al., 2014).

1.2 Coastal Flooding

Coastal Flooding is driven by storm surge and high-tide events. Currently, many coastal areas experience extreme water levels (EWLs) during high tides or large storms. At most locations globally, increasing mean sea level is the primary reason for increases in extreme water level (Menendez & Woodworth, 2010). Rising EWLs expose many areas to increased severity and frequency of coastal flooding, leading to the onset of chronic flooding conditions (Menendez & Woodworth, 2010; Merrifield et al., 2013; Vousdoukas et al., 2018). Areas with larger observed EWLs include the northwest shelf of Australia, western Europe, and western Canada and southern Alaska (Menendez & Woodworth, 2010; Merrifield et al., 2013). Areas with lower observed EWLS include the central and western Pacific Ocean and the Indian Ocean (Merrifield et al., 2013). The North Sea, the east coast of the US, and west and central Pacific are experiencing increasing trends in EWL, while Arctic North America, Alaska, and northwestern Australia are experiencing a decreasing trend in EWL (Menendez & Woodworth, 2010). Annual variation in EWL is defined by a combination of the predictable tidal cycle and nontidal residuals, of which the largest component is storm surge (Menendez & Woodworth, 2010; Merrifield et al., 2013; Muis et al., 2016).

Whether nontidal residuals drive coastal flooding depends on geographical and oceanographic characteristics of each location. In areas where extratropical storms are common, EWL tends to have higher contributions from nontidal residuals than high tides from the usual, predictable tidal cycle (Merrifield et al., 2013). Places where the EWL contribution from storm surge is large include the Southern Ocean, the North Pacific Ocean, the Atlantic Ocean, the Mediterranean Sea, the Gulf of Mexico, the Caribbean Sea, the Red Sea and the Sea of Japan (Merrifield et al., 2013). In parts of the North Pacific, Atlantic, and Southern Oceans, the tidal amplitude is naturally low due to proximity to tidal amphidromes, causing nontidal residuals to dominate EWLs in these

areas (Merrifield et al., 2013). Due to the standing-wave pattern of the tide in the tropics, tidal nodes and anti-nodes are relatively constant, leading to variation in tidal amplitude between islands in the western and central Pacific (Merrifield et al., 2013). As a result, some Pacific islands have low tidal amplitude and nontidal residuals contribute more to EWL (Merrifield et al., 2013). In places with shallow coastal areas, like the northwest coast of Australia, tidal range tends to be larger and EWL is due to high tides or a combination of high tides and storm surge (Merrifield et al., 2013). Annual maximum water levels on the western coast of North America, the marginal seas of Europe, and northern Australia tend to be more tidally driven than on the eastern coast of North America, the outer coasts of Europe, and the southern coast of Australia (Merrifield et al., 2013).

High tide related coastal flooding is increasing in frequency and severity. In past decades, most coastal flooding was caused by storm surge (Muis et al., 2016; Sweet et al., 2022). However, with rising sea levels, the frequency and severity of high-tide related flooding events is increasing (Buchanan et al., 2017; Sweet et al., 2022). From 2000 to 2020 in the northeastern US, occurrences of minor high-tide flooding increased from 5 days per year to 10 to 15 days per year (Sweet et al., 2022). In the southeastern US during the same timeframe, minor high tide flooding occurrences increased from 0 to 2 days per year to 5 to 10 days per year (Sweet et al., 2022). Locations where the contribution from high tides to EWL is high include the northwest shelf of Australia, the East coast of Africa, the eastern Pacific, and some Pacific islands (Merrifield et al., 2013). An increase in minor flooding due to sea level rise could be accompanied by increases in more damaging flooding during storms, especially when coinciding with high tide events (Menendez & Woodworth, 2010; Muis et al., 2016; Sweet et al., 2022).

1.3 Motivation

Coastal flooding threatens many locations globally. Many large cities currently threatened by coastal flooding have some structural flood defenses already in place, such as the construction of shoreline barriers (Cooper & Pile, 2014). However, rural areas and those with less commercial development and smaller population tend not to have physical flood barriers already in place, even if currently threatened by coastal flooding (Cooper & Pile, 2012). Flooding could damage roads and infrastructure, leading to closures (Strauss et al., 2012). High water levels could backflow through storm-water drainage systems, blocking storm-water drainage, and creating water obstacles on city streets and in low structures such as basements and parking lots (Titus et al., 1987). Trash and pollutants from areas inundated with water could pollute rivers, beaches, and the ocean when floodwaters recede, and cause negative health impacts to humans and wildlife (Trtanj et al., 2016).

In particular, small island states are among the most vulnerable to sea level rise related flooding (Leatherman & Beller-Simms, 1997). Many island nations are low-lying and have large coastlines compared to the total inland area (Leatherman & Beller-Simms, 1997). Many islands are susceptible to tropical storms, erosion, and have high populations living in coastal areas (Leatherman & Beller-Simms, 1997). In addition, freshwater is often scarce and is further threatened by saltwater intrusion into the water table (Leatherman & Beller-Simms, 1997). Island nations and individual small island states are isolated, and are reliant on the importation of resources needed to address flooding hazards (Leatherman & Beller-Simms, 1997).

Currently, 76 million people around the world live in the 1 in 100 year floodplain (Muis et al., 2016). Rare and extreme 1 in 100 years floods could cause severe damage and threaten the safety and homes of people living in hazardous floodplains. However, minor but frequent flooding could cause more long-term and consistent damage,

requiring persistent maintenance. As sea level rise increases, minor high tide flooding will become more frequent and affect more locations globally (Menendez & Woodworth, 2010; Thompson et al., 2021). Therefore, planning for frequent and minor flooding events in addition to extreme events is vital in protecting coastal communities from the effects of increasing sea level and flooding. While there has been some discussion on flooding and chronic flooding in individual locations, such as variation across the United States, there has not been a quantitative study of the transition from occasional to chronic flooding on a global scale.

The goal of this study is to quantify and understand global differences in the transition from occasional to chronic coastal flooding. We first determine the amount of sea-level rise needed at each location to produce the transition, which distinguishes locations where the transition is expected to occur rapidly from locations where the transition is expected to occur at a slower rate. Based on future sea-level rise scenarios, we then quantify the duration of the transition period and demonstrate how the transition period changes in time as the rate of sea-level rise increases. Finally, we identify the characteristics of local water-level variability that lead to location-based differences in transition time.

2.0 METHODS

2.1 Selecting Tide Gauges

Hourly time series of sea level from a globally distributed set of tide gauges were used in order to quantify the transition from occasional to chronic flooding (Figure 1). Tide gauge data were obtained from the University of Hawaii Sea Level Center (UHSLC) Fast Delivery Tide Gauge Dataset. To be included, selected tide gauge records were required to be longer than 20 years, with an annual data return of more than 320 days (Figure 1). The 320-day threshold was used to exclude individual years in the tidal record, but in the case that excluding those years reduced the valid number of years to less than 20, the tidal-record for that location was excluded as well.

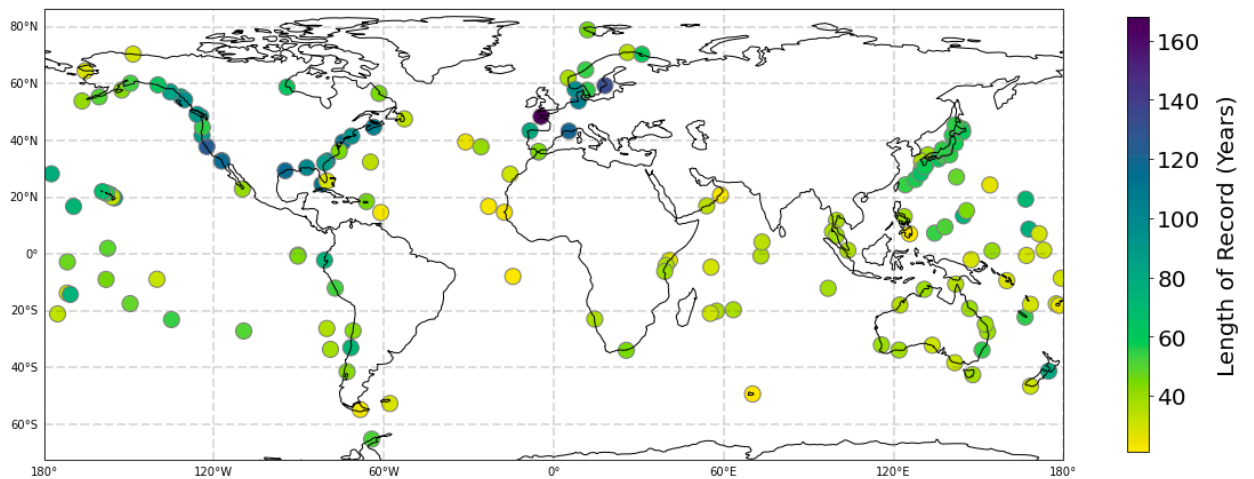


Figure 1. Locations of selected tide gauges and length of record at each location

2.2 Determining Transition From Occasional To Chronic

2.2.1 Required Sea-Level Rise

In order to determine the amount of sea-level rise required to produce a transition from occasional to chronic flooding in each location, we first produced a detrended time series for each tide gauge by subtracting a linear trend obtained using least-squares regression from the hourly time series. Daily maxima were then extracted

from each detrended time series. Next, we iterated over thresholds in increments of 1 cm between $\frac{1}{2}$ the standard deviation of the detrended time series and the maximum value of the detrended time series. For each location and threshold, we tabulated the number of daily maxima exceeding the threshold in each meteorological year (defined to be May–April to avoid splitting the winter and summer storm seasons) and calculated the mean number of exceedances across the years in each record. For each location, we defined the occasional flooding threshold (T_{occ}) and chronic flooding threshold (T_{chr}) to be the lowest thresholds for which the average number of exceedances is greater than 1 and 20, respectively. Examples from the Honolulu, HI and Newport, RI tide-gauge records demonstrate how the thresholds relate to the time series of daily maxima extracted from the detrended hourly water levels (Figure 2).

It is important to note that since these thresholds were defined relative to the detrended time series, the relationship to tidal datums is removed, and the heights of the thresholds are not meaningful in of themselves. There is a continuum of thresholds between T_{chr} and T_{occ} that are relevant for different elevations, and each threshold will experience the transition at different times. However, the effect of SLR on the frequency of flooding can be visualized by considering that any flooding threshold of interest will be closer to mean sea level in the future as the mean water level rises (Figure 2). Thus, subtracting T_{occ} from T_{chr} represented the change in sea level (Δh) required to produce a transition from occasional flooding (1 day per year on average) to chronic flooding (20 days per year on average) (Figures 2 & 3). The fact that T_{chr} was lower than T_{occ} indicated that the T_{occ} represents sea-level conditions further in the future compared to the T_{chr} .

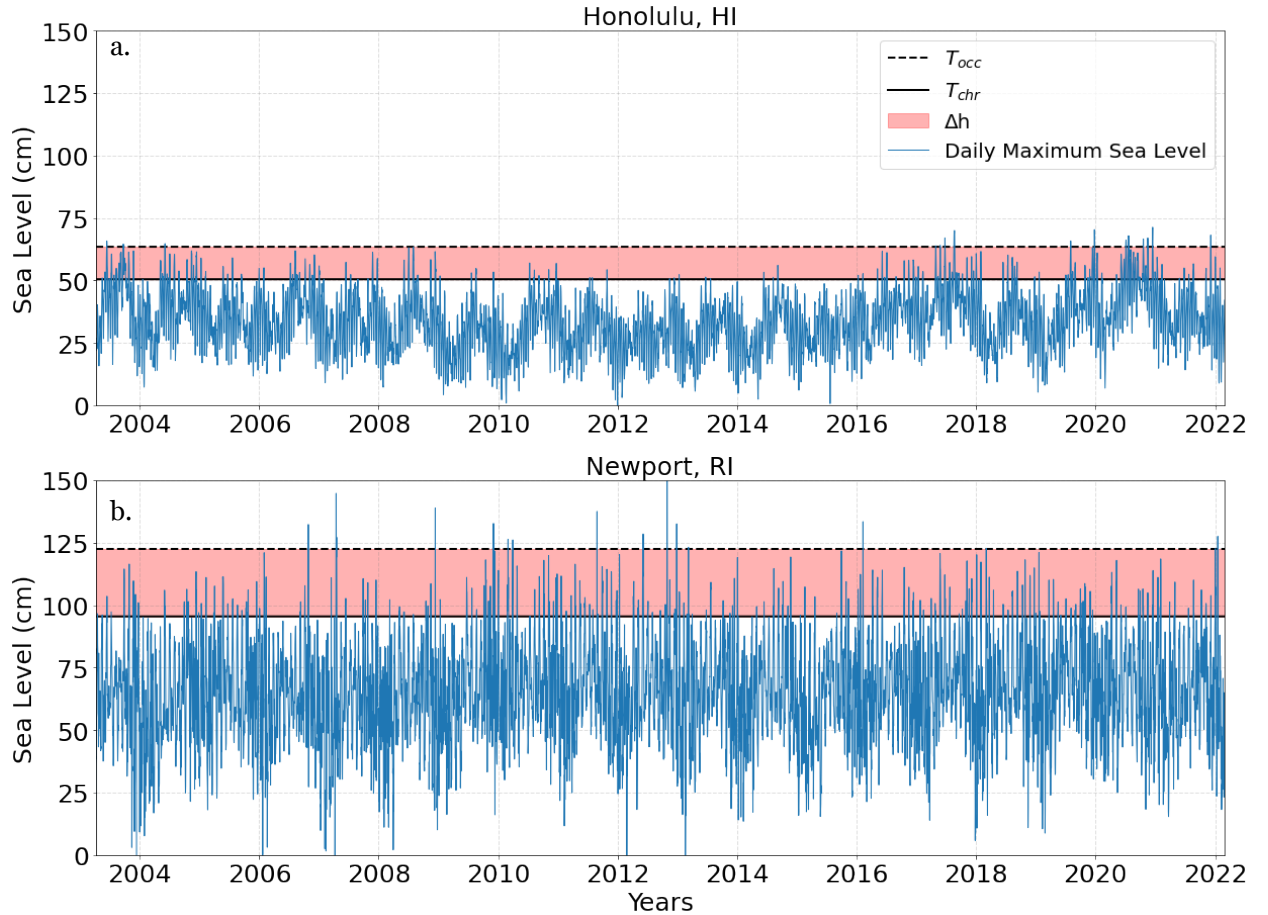


Figure 2. Daily maximum sea level from detrended hourly tide gauge records in (a.) Honolulu, HI, and (b.) Newport, RI. The chronic flooding threshold (T_{chr}) and occasional flooding threshold (T_{occ}) are depicted by the straight and dashed black lines, respectively. The difference between the two thresholds is the required sea level rise to transition to a chronic flooding regime (Δh).

The purpose of this analysis was to determine the difference between the two thresholds (Δh), not the height of the thresholds themselves. Since Δh depends only on the statistics of sea-level variability at each location, we made the assumption that the variability at each location will not change significantly into the future. Because the thresholds are defined arbitrarily based on the number of exceedances in the current record, what may be relevant now could differ from what may be relative to higher elevations along the coast as the threshold rises. Therefore, detrending the time series and thus removing the mean and relevance to a specific date did not affect the value of Δh .

2.2.2 Transition Timeline

To establish the timeline of potential transitions under different sea-level rise scenarios, we use the "Gridded projections for the interagency report: Global and Regional Sea Level Rise Scenarios for the United States: Updated Mean Projections and Extreme Water Level Probabilities Along U.S. Coastlines" (Sweet et al., 2022; [<https://zenodo.org/record/6067895#.ZCJkXi-B2gQ>]). These scenarios were provided with decadal resolution, which we interpolated to annual resolution with a cubic spline. For each scenario and each tide gauge, we identified the integer number of years required for sea-level rise equivalent to Δh to occur, i.e., the transition time (Δt). Because the rate of sea-level rise changed in time, we performed this analysis for two different starting years—2020 and 2050—resulting in one transition for the first half of the 21st century (Δt_{2020}) and one for the second half (Δt_{2050}), where the subscript denotes the starting year (Figure 5). Towards the latter half of the century, rates of sea level rise tend to increase significantly, so we performed the second analyses starting in 2050 to explore how transition times will differ starting at this later date. The intermediate low, intermediate, and intermediate high scenarios were all considered when calculation transition time, although we focus primarily on results using the intermediate scenario. For the intermediate scenario, GMSL was projected to rise 23.00 cm by 2050, and 82.24 cm by 2100. Considering the intermediate-low scenario, GMSL was projected to rise 15.51 cm by 2050, and 28.46 cm by 2100. Finally, using the intermediate-high scenario, GMSL was projected to rise 28.23 cm by 2050, and 118.95 cm by 2100. Regional variability will cause the projected sea level to differ from the GMSL by location.

2.3 Non-Tidal Residuals

The predicted tide for each tide gauge location was calculated using the Unified Tidal Analysis and Prediction (Utide) python package, using the most recent 20 years of the detrended hourly time series for each location (<https://github.com/wesleybowman/UTide>). The predicted tide for each location was reconstructed using the 68 default constituents as defined by Utide, and standard nodal and satellite corrections were made. Subtracting the tide prediction from the observed detrended time series returned the nontidal residuals for each location.

3.0 RESULTS

3.1 Required Sea Level Rise

The smallest Δh values were found in islands and lower latitudes. The correlation between Δh and standard deviation of the predicted tide was 0.49, and the correlation between Δh and the standard deviation of the standard deviation of the non-tidal residuals was 0.89 (Figure 4). This relationship indicates that Δh tends to be more driven by non-tidal residuals than the high tides related to the predictable tidal cycle. The correlation between both non-tidal residuals and the predicted tide with Δh was expected to be larger than the correlation with Δt , because the Δt considers regional differences in sea level rise that are not represented by Δh (Figure 6).

Some of the largest expected Δh values, such as those in Alaska, Australia, and Northern Europe, are in higher latitudes, heavily glaciated areas, or in the case of Australia, on a shallow continental shelf. The global median Δh was 20.0 +/- 14.06 cm (Appendix: Table 2). The median for continental locations was 26.0 +/- 14.70 cm, and the median for island locations was 15.0 +/- 9.32 cm. Only islands and East Africa have less than the global median Δh (Appendix: Table 2). The median Δh for East Africa was 19.5 +/- 10.44 cm (Appendix: Table 2). The highest median Δh was found in west North America, where the median Δh was 39.50 +/- 14.27 cm (Appendix: Table 2), which was primarily due to large Δh values along Alaskan and Canadian coastlines.

By latitude, Δh tends to decrease toward lower latitudes (Appendix: Table 2). Δh is less than the global median between 40°S and 20°N, with the lowest median and lowest variability of Δh found in the 0° to 20°N range with a value of 15.0 +/- 4.73 cm (Appendix: Table 2). The highest median values for Δh were found between 60°N and 80°N, with a median of 37.0 +/- 15.52 cm (Appendix: Table 2).

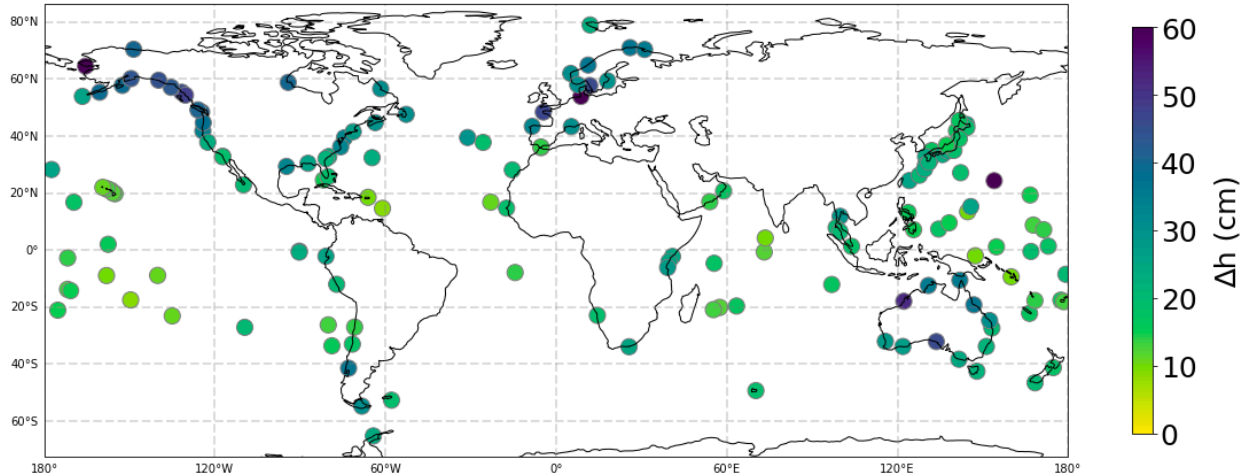


Figure 3. Sea-level rise needed for transition from T_{occ} to T_{chr} (Δh).

The smallest Δh values were found in islands and lower latitudes. The correlation between Δh and standard deviation of the predicted tide was 0.49, and the correlation between Δh and the standard deviation of the standard deviation of the non-tidal residuals was 0.89 (Figure 4). This relationship indicates that Δh tends to be more driven by non-tidal residuals than the high tides related to the predictable tidal cycle. The correlation between both non-tidal residuals and the predicted tide with Δh was expected to be larger than the correlation with Δt , because the Δt considers regional differences in sea level rise that are not represented by Δh (Figure 6).

Some of the largest expected Δh values, such as those in Alaska, Australia, and Northern Europe, are in higher latitudes, heavily glaciated areas, or in the case of Australia, on a shallow continental shelf. The global median Δh was 20.0 +/- 14.06 cm (Appendix: Table 2). The median for continental locations was 26.0 +/- 14.70 cm, and the median for island locations was 15.0 +/- 9.32 cm. Only islands and East Africa have less than the global median Δh (Appendix: Table 2). The median Δh for East Africa was 19.5 +/- 10.44 cm (Appendix: Table 2). The highest median Δh was found in west North America, where the median Δh was 39.50 +/- 14.27 cm (Appendix: Table 2), which was primarily due to large Δh values along Alaskan and Canadian coastlines.

By latitude, Δh tends to decrease toward lower latitudes (Appendix: Table 2). This latitudinal dependence is likely due to increased storminess towards the poles. Δh was less than the global median between 40°S and 20°N , with the lowest median and lowest variability of Δh found in the 0° to 20°N range with a value of 15.0 ± 4.73 cm (Appendix: Table 2). The highest median values for Δh were found between 60°N and 80°N , with a median of 37.0 ± 15.52 cm (Appendix: Table 2).

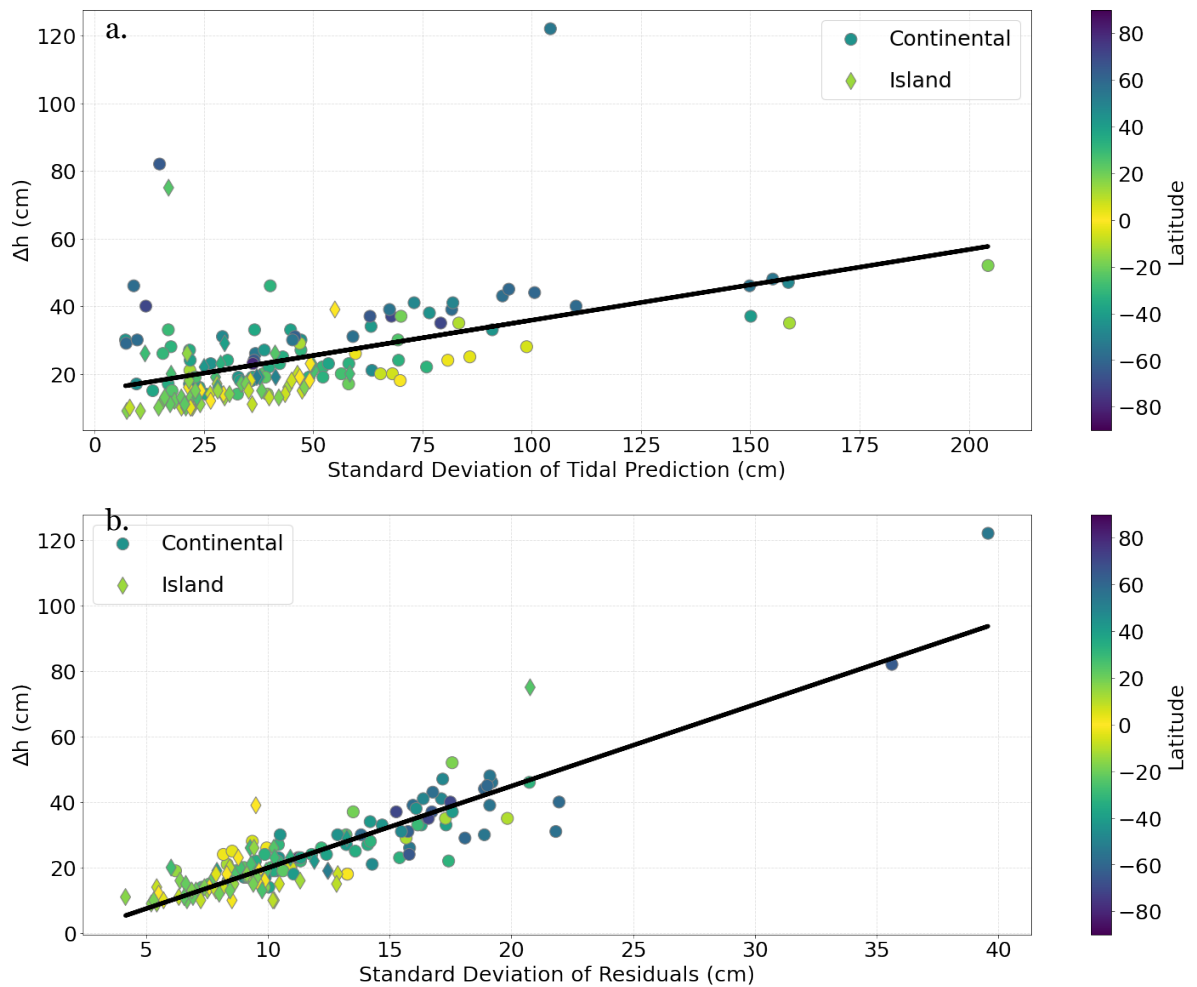


Figure 4. Correlation between (a.) STD of predicted tide and (b.) STD of NTRs, and Δh . Black line: Correlation for all locations.

3.2 Transition Timeline

The Δt_{2020} and Δt_{2050} values range from 0 years to 130 years for the intermediate low, intermediate, and intermediate high scenarios. Starting in 2020, the global mean for the intermediate scenario across all locations was 35.71 years and the global median for the intermediate scenario was 31.0, with a standard deviation of 17.28 years. As sea level continues to rise, higher elevations will be impacted and similar transitions will occur for higher thresholds throughout the century, that could impact a larger land area. We also considered the transition time starting in 2050 to capture the changes in these higher thresholds. Starting in 2050, the expected transition times decrease globally and regionally. Global mean transition time for the intermediate scenario was 22.86 years, and median global transition time was 20 years with a standard deviation of 14.06 years. Transition times vary from the global mean and median based on location.

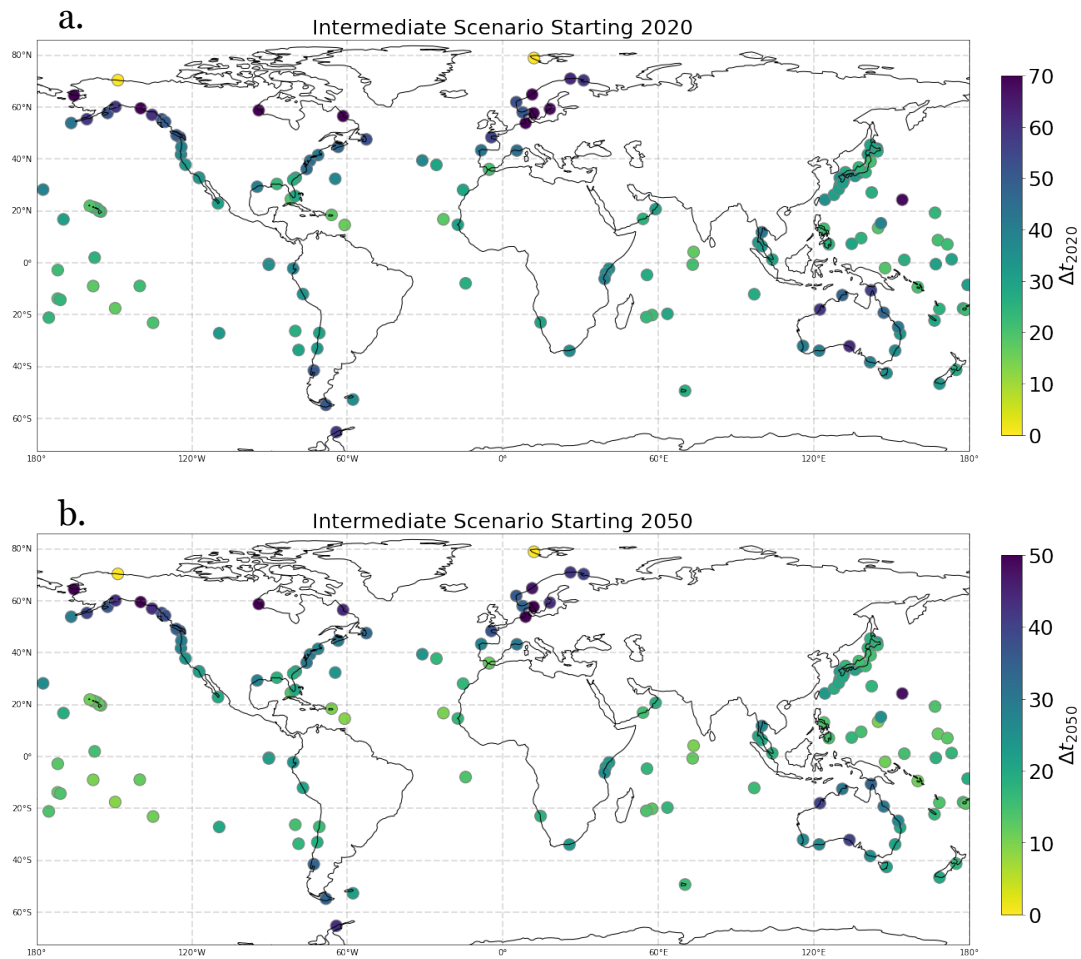


Figure 5. (a.) Number of years transition time to T_{chr} starting in 2020 (Δt_{2020}).
(b.) Number of years transition time to T_{chr} starting in 2050 (Δt_{2050}).

Europe, Western North America, and Australia are projected to have regionally larger transition times than the global median, which will be explored further in the following sections. For intermediate scenarios starting in 2020, Northern Europe had the largest median transition time, ranging from 0 to 101 years with a median of 62.0 ± 25.38 years, which is equivalent to about an 100% increase from the global intermediate scenario median transition time (Table 1). The Northwest coast of North America, including Oregon, Washington, British Columbia, and Alaska also have longer transition times on average, but vary considerably (Table 1). The Δt_{2020} value in Southwest North America tends to be closer to the global median, leading to the largest range of transition

times in West North America, with a median above the global median and large standard deviation. Intermediate transition times in Western North America range from 0 years to 130 years, with a median of 49.5 +/- 24.95 years (Table 1). In Prudhoe Bay, AK, sea level was projected to decline under every emissions scenario, so an increase in flooding was unexpected and the transition time was therefore 0 years. In Nylesund, the projected sea level follows a similar negative trend, leading to a default transition time of 0 years in order to avoid negative values. Intermediate projected transition times in Australasia are also longer than the global median, but are less variable. The median transition time in Australasia was 37.5 +/- 11.99 years, or about 20.97% larger than the global median transition time (Table 1). The median transition time for East Asia was 3.2% lower than the global median, with a regional median transition time of 30.0 +/- 4.83 years (Table 1).

For intermediate scenario transition times starting in 2050, the distribution of regions with greater median transition times, like Europe, and lower median transition times, like islands, remained similar. Regional and global median transition times starting in 2050 decrease significantly, with the global median decreasing by 35%, the median for Northern Europe decreasing by 32.2%, and the median for islands decreasing by 40%.

Table 1. Median transition time by region and start year

Region	2020 Start		2050 Start	
	Median Transition Time (Years)	STD Transition Time (Years)	Median Transition Time (Years)	STD Transition Time (Years)
Islands	25.0	9.052510	15.0	6.469519
West North America	49.5	24.948404	35.0	23.233716
East North America	42.0	20.426807	28.0	12.655190
Northern Europe	62.0	25.376182	42.0	25.534774
East Atlantic	29.5	11.279822	17.5	8.231039
East Asia	30.0	4.835674	19.0	3.166459
Australasia	37.5	11.989836	23.0	8.458322
East Africa	36.0	4.913134	23.0	3.547299
West South America	38.0	10.466662	24.0	9.129454
Continents	37.5	19.041686	24.5	16.047880

3.2.1 Non-Tidal Residuals

High water levels can occur due to high tides in the tidal cycle, storm surge, or a combination of both. To investigate the contributing factors to transition height and transition time, we compare the non-tidal residuals and predicted tide for each tide gauge location. Overall, transition time had a higher correlation to the standard deviation of nontidal residuals than the standard deviation of the predicted tide. The correlation between the standard deviation of the nontidal residuals and intermediate scenario transition time was the strongest, at 0.84 (Figure 6b). Standard deviation of predicted tide

and intermediate scenario transition time show a weak positive correlation of 0.42 (Figure 6a). When locations above 40°N and below 40°S are removed, the correlation between the standard deviation of the non-tidal residuals and transition time weakens and becomes 0.75. Conversely, the correlation between predicted tide and transition time becomes stronger, at 0.5. This relationship could indicate that normal tidal cycle contributes more to Δh at high latitude locations than the non-tidal residuals.

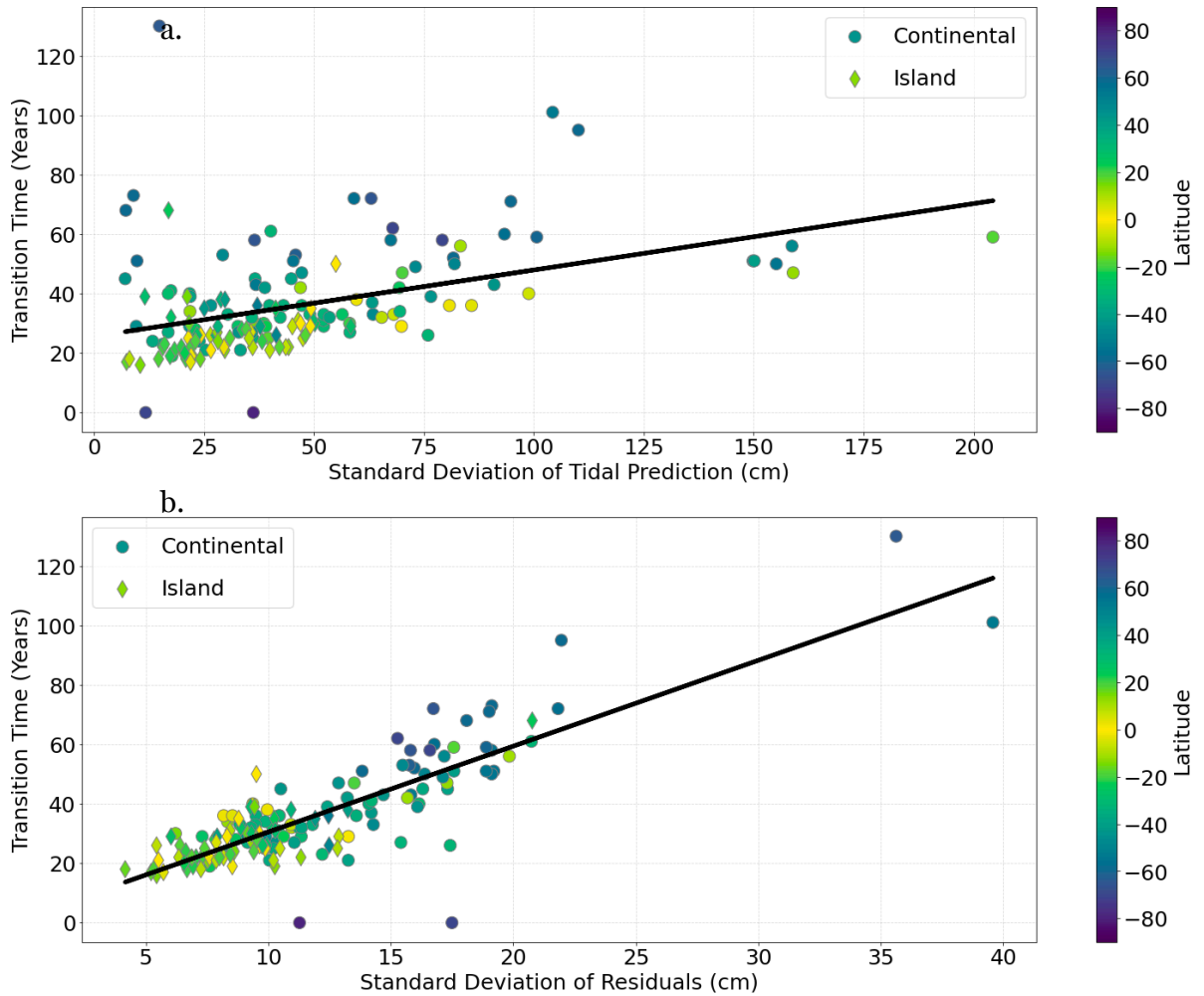


Figure 6. Correlation between (a.) STD of predicted tide and (b.) STD of NTRs, and transition time. Black line: Correlation for all locations.

The longest projected transition time was 130 years, found in Nome, AK, where the intermediate scenario standard deviation of the nontidal residuals was 35.63 cm,

247% higher than the global median standard deviation of nontidal residuals. The lowest projected transition time above 0 was 16 years in Fort-de-France, Martinique. Standard deviation of nontidal residuals in Fort de France was 5.44 cm, which was 47% lower than the global median. All of the 11 lowest transition times, all under 20 years for the intermediate scenario, are located on islands, and below the global median standard deviation of non-tidal residuals.

3.2.2 Islands and Continents

Islands in general have shorter projected transition times with less variability (Figure 7a). Island transition times range from 16 years to 68 years and average 26.625 +/- 8.36 years, which was about 19.35% shorter than the global median intermediate scenario transition time and 33.33% lower than median intermediate scenario transition time for continental locations (Figure 7). Compared to continental coasts, projected transition times for island locations tend to be shorter for all scenarios.

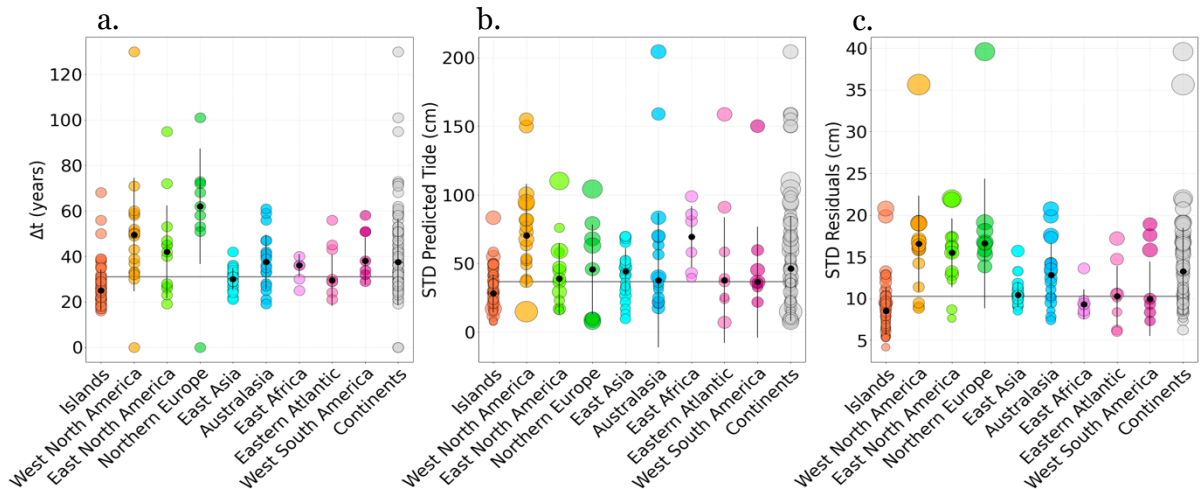


Figure 7. Regional and island distribution of (a.) transition time, (b.) standard deviation of predicted tide, and (c.) standard deviation of nontidal residuals. Size of markers corresponds to Δt_{2020} for the intermediate scenario.

3.2.3 Latitude

Median projected transition time also varies with latitude. Higher latitudes tend to have longer projected transition times than lower latitudes, as transition time increases with distance from the equator. Grouped in 20° sections, locations within latitudes from 40°S to 40°N have shorter mean transition times than the global average (Figure 8a). The median standard deviation of the predicted tide, without nontidal residuals, was also below the global median of 36.84 +/- 32.80 cm for locations within latitudes from 40°S to 40°N (Figure 8b). Locations between 0° to 20°N had the lowest median transition time and the least variation, with an intermediate scenario median of 25.0 years and a standard deviation of 6.47 years (Figure 8a). Between 0° to 20°N, the median standard deviation of the nontidal residuals, about 9.54 +/- 2.75 cm, and the median standard deviation of the predicted tide, about 35.95 +/- 16.42 cm, are both low relative to other latitudes and below the global median (Figure 7bc). In comparison, the median standard deviation of the predicted tide for latitudes 20°S to 0°N was larger than the global median, but the median standard deviation of the nontidal residuals was slightly lower than the equivalent latitudes in the Northern hemisphere, resulting in a longer median transition time of 27 +/- 11.31 years for the intermediate scenario (Figure 8abc).

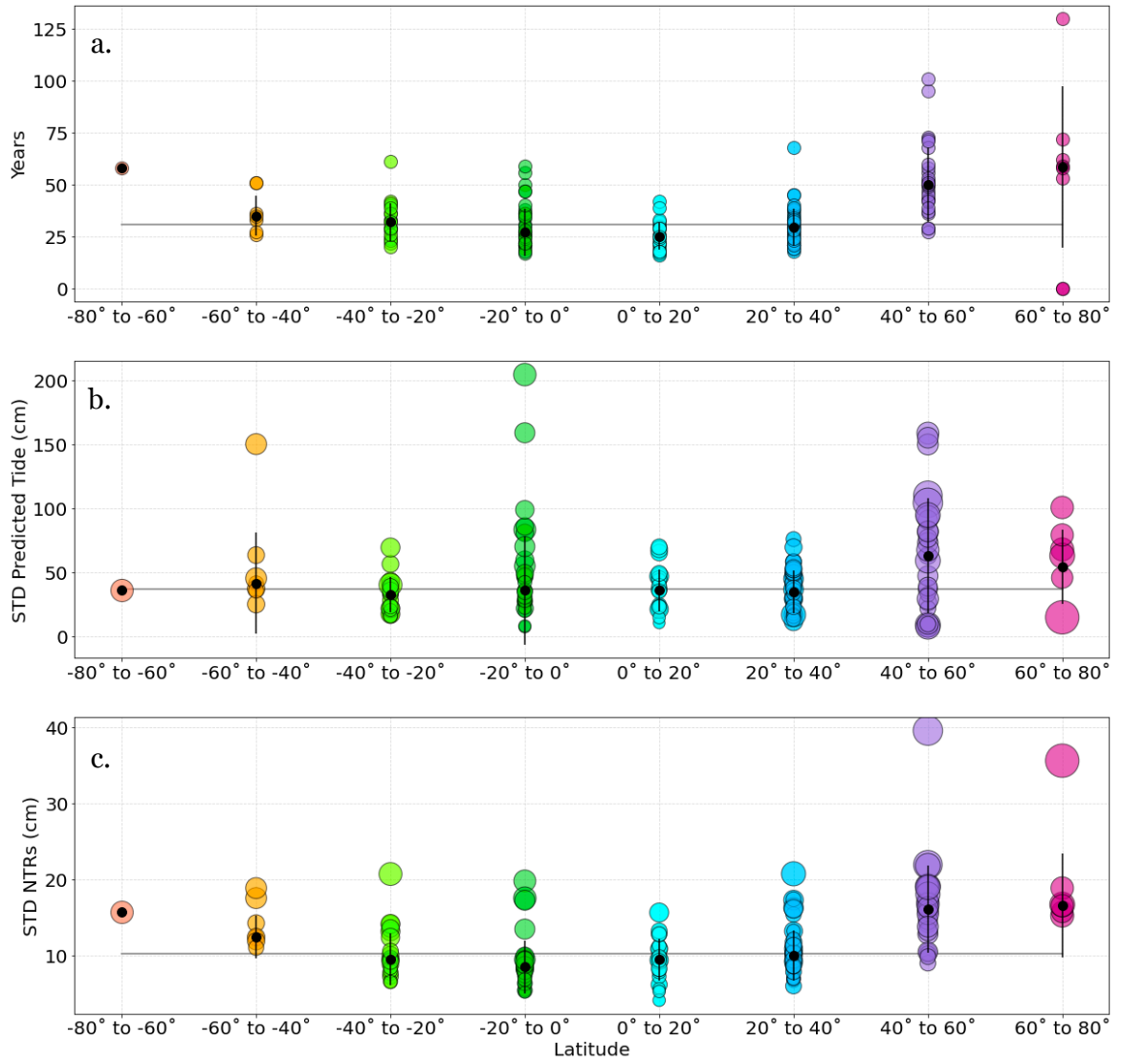


Figure 8. Distribution by latitude of (a.) t_{2020} , (b.) STD of predicted tide, and (c.) STD of non-tidal residuals

4.0 DISCUSSION

As GMSL rises, flooding in many places is expected to increase (Vousdoukas et al., 2018; Menendez & Woodworth, 2010). In many areas, occasional flooding is already occurring (Vousdoukas et al., 2018; Menendez & Woodworth, 2010). With rising GMSL, occasional flooding is expected to increase in severity and frequency, giving less time between events to repair damage and mitigate negative effects of flooding (Vousdoukas et al., 2018; Strauss et al., 2012). Regionally, the speed of the transition to chronic flooding varies.

In general, islands are most vulnerable to increasing frequency of flooding at high tide, which as a group average lower than the global median for transition times and the median transition time for continental locations (Leatherman & Beller-Simms, 1997). This is due to the fact that islands tend to have smaller tidal ranges on average than most continental locations, and the median STD of non-tidal residuals for islands was also lower than the global median and the median for continental locations. A smaller range between high and low tide, and lower sea level height difference from storm surge suggests that high water levels in island locations are more consistent, and the frequency of flooding will be impacted more by rising sea levels than increasing storms or extreme high tides. For example, in Honolulu, HI, the tidal range is small leading to a lower Δh (12.0 cm) and Δt_{2020} (21 years) compared to Newport, RI, where the tidal range is larger, resulting in higher Δh (27.0 cm) and Δt_{2020} (42.0 years) values (Figure 2).

The most vulnerable region is Eastern Asia, which also consists of the most island locations within a region. Although not as extreme as islands as a group, the median transition times for Eastern Asia are projected to be lower than the global median. The STD of the predicted tide is greater than the global median while the STD of non-tidal residuals is lower. This could suggest that high water events are more driven by high tides and less so by storm surge in Eastern Asia (Muis et al., 2016; Merrifield et al.,

2013). However, there is high variability within every region, especially Northern Europe, Western North America, and Australia. Due to low concentration of long-standing tide gauges in South America and Africa, there is less available data despite the geographical size of these regions. As the length of the tidal record increases in these locations, a less euro-centric regional analysis could be better accomplished. Further studies should calculate the standard deviation of the daily maximum tide, instead of the entire tidal range for each location, as the STD of the entire predicted tide does not distinguish between tides with consistent highs in diurnal or semi-diurnal cycles, and mixed tides with more variability in daily maximums.

Beyond the scope of this study is the nodal cycle, which consists of changes in tides on decadal timescales (Thompson et al., 2021). Taking into account these changes could alter the projected transition times for certain locations (Thompson et al., 2021). With further changes in climate, we are also likely to see changes in storm frequency and severity, which may alter the relationship between non-tidal residuals and the predicted tidal cycle (Merrifield et al., 2013). Finally, the global projections used to estimate transition time from total projected sea level rise predicted a declining trend in locations like Nome, Alaska, due to vertical land motion and glacial retreat (Larsen et al., 2005). As glaciers continue to melt and the elastic response of the land decreases, this may change to an increasing trend in sea level height and alter the projected transition times (Larsen et al., 2005).

Overall, these transition times form a basis for a timeline that may help to predict and prepare for chronic flooding. The T_{chr} corresponds to a mean 20 days of maximum threshold exceedances, which could reflect a range of 10 - 40 days of flooding in an individual year. The regional differences in the timeline illustrate the need for region-specific mitigation and planning and the need for more urgent preparation in vulnerable places like islands (Leatherman & Beller-Simms, 1997). Ideally, locations with the

shortest transition times should begin to prepare for and address chronic flooding conditions well before the projected transition time has elapsed.

APPENDIX A: Tables

Table 2. Median transition time by region and start year

Region	Median Transition Time (Years)	STD Transition Time (Years)	Median STD of Predicted Tide (cm)	STD of Predicted Tide STD (cm)	Median STD of Non-Tidal Residuals	STD of Non-Tidal Residual STD
Islands	25.0	9.05	28.20	13.87	8.53	2.88
West North America	49.5	24.95	70.31	37.69	16.58	5.76
East North America	42.0	20.43	38.86	26.02	15.49	4.11
Northern Europe	62.0	25.376182	45.861859	32.555515	16.599017	7.769126
East Atlantic	29.5	11.279822	37.850266	45.802012	10.280512	3.629040
East Asia	30.0	4.83	44.27	17.03	10.44	1.54
Australasia	37.5	11.989836	37.899251	48.911334	12.816569	3.820788
East Africa	36.0	4.913134	69.487931	22.216551	9.302018	1.786041
West South America	38.0	10.466662	36.532219	40.465289	9.962422	4.450505
Continents	37.5	19.04	46.41	38.23	13.27	5.21

Table 3. Median transition time, STD of predicted tide, and STD of non-tidal residuals by latitude

Latitude	Required SLR (Δh) (cm)	Median Transition Time (Years)	Median STD of Predicted Tide (cm)	Median STD of Non-tidal Residuals (cm)
60°S to 40°S	24.0 +/- 0.00	35.0 +/- 9.52	41.46 +/- 39.55	12.49 +/- 2.79
40°S to 20°S	21.0 +/- 6.58	32.0 +/- 9.25	32.74 +/- 13.99	9.54 +/- 3.38
20°S to 0°	19.0 +/- 8.15	27.0 +/- 11.32	36.10 +/- 42.27	8.53 +/- 3.48
0° to 20°N	17.0 +/- 10.34	25.0 +/- 6.48	35.95 +/- 16.42	9.54 +/- 2.75
20°N to 40°N	15.0 +/- 4.73	29.5 +/- 9.07	34.73 +/- 16.67	9.99 +/- 3.30
40°N to 60°N	20.5 +/- 10.22	50.0 +/- 17.74	63.28 +/- 44.82	16.09 +/- 5.71
60°N to 80°N	34.0 +/- 18.86	58.5 +/- 38.79	54.45 +/- 29.08	16.67 +/- 6.81

APPENDIX B: Figures

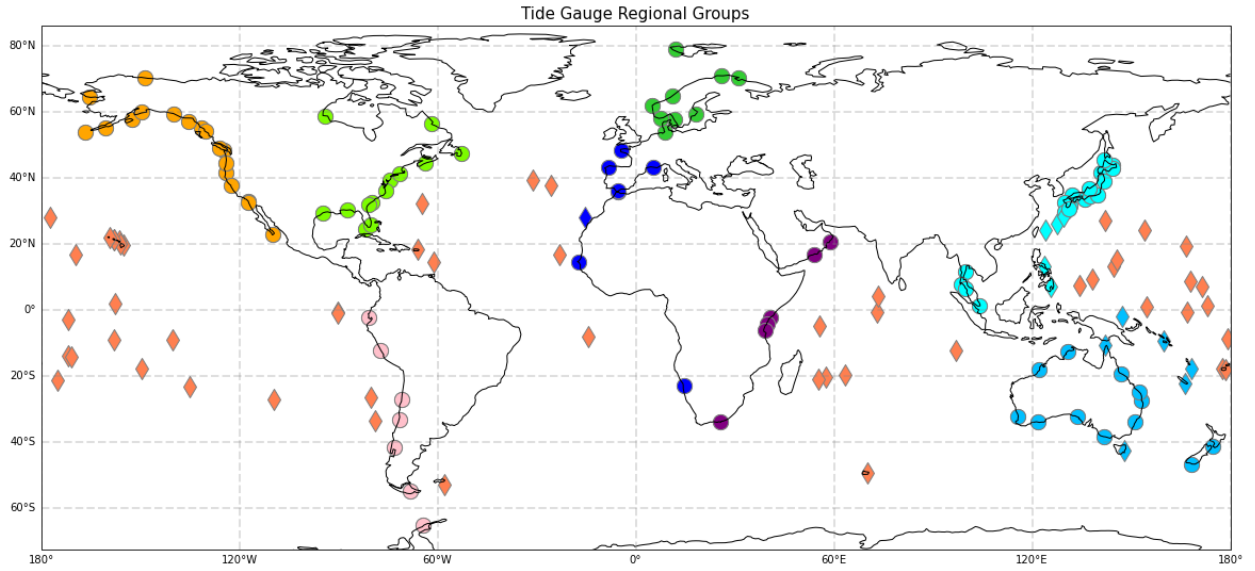


Figure 9. Tide Gauges separated into regions. (Circle shape): Continents; Orange: Western North America; Lime Green: Eastern North America; Dark Green: Northern Europe; Cyan: Eastern Asia; Blue: Australasia; Coral (diamond shape): Islands

REFERENCES

- Buchanan, M.K., M. Oppenheimer, and R.E. Kopp, 2017: Amplification of flood frequencies with local sea level rise and emerging flood regimes. *Environmental Research Letters*, 12 (6), 064009. <https://doi.org/10.1088/1748-9326/aa6cb3>
- Caldwell, P. C., M. A. Merrifield, P. R. Thompson (2015), Sea level measured by tide gauges from global oceans — the Joint Archive for Sea Level holdings (NCEI Accession 0019568), Version 5.5, NOAA National Centers for Environmental Information, Dataset, doi:10.7289/V5V40S7W.
- Cooper, J. A. G. & Pile, J, 2014: The adaptation-resistance spectrum: a classification of contemporary adaptation approaches to climate-related coastal change. *Ocean and Coastal Management*, 94, 90–98.
<https://doi.org/10.1016/j.ocecoaman.2013.09.006>
- Frederikse, T., F. Landerer, L. Caron, S. Adhikari, D. Parkes, V.W. Humphrey, S Dangendorf, P. Hogarth, L. Zanna, L. Cheng, Y. Wu, 2020: The causes of sea-level rise since 1900. *Nature* 584, 393–397. <https://doi.org/10.1038/s41586-020-2591-3>
- Kopp, R.E., R.M. Horton, C.M. Little, J.X. Mitrovica, M. Oppenheimer, D.J. Rasmussen, B.H. Strauss, and C. Tebaldi, 2014: Probabilistic 21st and 22nd century sea-level projections at a global network of tidegauge sites. *Earth's Future*, 2 (8), 383–406.
<https://doi.org/10.1002/2014EF000239>
- Krasting, J.P., J.P. Dunne, R.J. Stouffer, and R.W. Hallberg, 2016: Enhanced Atlantic sea-level rise relative to the Pacific under high carbon emission rates. *Nature Geoscience*, 9 (3), 210–214. <http://dx.doi.org/10.1038/ngeo2641>
- Gregory, J.M., Griffies, S.M., Hughes, C.W. et al., 2019: Concepts and Terminology for Sea Level: Mean, Variability and Change, Both Local and Global. *Surveys in Geophysics*, 40, 1251–1289. <https://doi.org/10.1007/s10712-019-09525-z>

- Larsen, C. F., R. J. Motyka, J. T. Freymueller, K. A. Echelmeyer, and E. R. Ivins, 2005: Rapid viscoelastic uplift in southeast Alaska caused by post-Little Ice Age glacial retreat. *Earth and Planetary Science Letters*, 237(3–4), 548– 560, doi:10.1016/j.epsl.2005.06.032.
- Leatherman, S. P., & Beller-Simms, N. 1997: SEA-LEVEL RISE AND SMALL ISLAND STATES: AN OVERVIEW. *Journal of Coastal Research*, 1–16. <http://www.jstor.org/stable/25736084>
- Menéndez, M., and P.L. Woodworth, 2010: Changes in extreme high water levels based on a quasi-global tide-gauge data set. *Journal of Geophysical Research: Oceans*, 115, C10011. <https://doi.org/10.1029/2009JC005997>
- Merrifield, M.A., A.S. Genz, C.P. Kontoes, and J.J. Marra, 2013: Annual maximum water levels from tide gauges: Contributing factors and geographic patterns. *Journal of Geophysical Research: Oceans*, 118 (5), 2535–2546. <https://doi.org/10.1002/jgrc.20173>
- Miller, K. G., R. E. Kopp, B. P. Horton, J. V. Browning, and A. C. Kemp, 2013: A geological perspective on sea-level rise and its impacts along the U.S. mid-Atlantic coast, *Earth's Future*, doi:10.1002/2013EF000135.
- Muis, S., M. Verlaan, H.C. Winsemius, J.C.J.H. Aerts, and P.J. Ward, 2016: A global reanalysis of storm surges and extreme sea levels. *Nature Communications*, 7 (1), 11969. <http://dx.doi.org/10.1038/ncomms11969>
- Strauss, B. H., Ziemiński, R., Weiss, J. L. & Overpeck, J. T, 2012: Tidally adjusted estimates of topographic vulnerability to sea level rise and flooding for the contiguous United States. *Environmental Research Letters*, 7, 14033.
- Sweet, W.V., B.D. Hamlington, R.E. Kopp, C.P. Weaver, P.L. Barnard, D. Bekaert, W. Brooks, M. Craghan, G. Dusek, T. Frederikse, G. Garner, A.S. Genz, J.P. Krasting,

- E. Larour, D. Marcy, J.J. Marra, J. Obeysekera, M. Osler, M. Pendleton, D. Roman, L. Schmied, W. Veatch, K.D. White, and C. Zuzak, 2022: Global and Regional Sea Level Rise Scenarios for the United States: Updated Mean Projections and Extreme Water Level Probabilities Along U.S. Coastlines. NOAA Technical Report NOS O1. National Oceanic and Atmospheric Administration, National Ocean Service, Silver Spring, MD, 111 pp.
<https://oceanservice.noaa.gov/hazards/sealevelrise/noaa-nostechrpt01-global-regional-SLR-scenarios-US.pdf>
- Thompson, P.R., M.J. Widlansky, B.D. Hamlington, M.A. Merrifield, J.J. Marra, G.T. Mitchum, and W. Sweet, 2021: Rapid increases and extreme months in projections of United States high-tide flooding. *Nature Climate Change*, 1–7.
<https://doi.org/10.1038/s41558-021-01077-8>
- Trtanj, J., L. Jantarasami, J. Brunkard, T. Collier, J. Jacobs, E. Lipp, S. McLellan, S. Moore, H. Paerl, J. Ravenscroft, M. Sengco, and J. Thurston, 2016: Chapter 6: Climate impacts on water-related illness. The impacts of climate change on human health in the United States: A scientific assessment. U.S. Global Change Research Program. <https://health2016.globalchange.gov>.
- Titus, J. G., C.Y. Kuo, M.J. Gibbs, T.B. LaRoche, M.K. Webb, J.O. Waddell, 1987: Greenhouse effect, sea level rise, and coastal drainage systems. *Journal of Water Resources Planning and Management*, 113(2), 216–227.
<http://papers.risingsea.net/downloads/sea-level-rise-coastal-drainage.pdf>
- Vousdoukas, M.I., L. Mentaschi, E. Voukouvalas, M. Verlaan, S. Jevrejeva, L.P. Jackson, and L. Feyen, 2018: Global probabilistic projections of extreme sea levels show intensification of coastal flood hazard. *Nature Communications*, 9 (1), 2360.
<http://dx.doi.org/10.1038/s41467-018-04692-w>